Static and dynamic friction in sliding colloidal monolayers

Andrea Vanossi [*] [†], **Nicola Manini** [‡] [†] [*] **and Erio Tosatti** [†] [*] [§]

[*]CNR-IOM Democritos National Simulation Center, Via Bonomea 265, 34136 Trieste, Italy,[†]International School for Advanced Studies (SISSA), Via Bonomea 265, 34136 Trieste, Italy,[‡]Dipartimento di Fisica, Università degli Studi di Milano, Via Celoria 16, 20133 Milano, Italy, and [§]International Center for Theoretical Physics (ICTP), Strada Costiera 11, 34104 Trieste, Italy

Submitted to Proceedings of the National Academy of Sciences of the United States of America

arXiv:1208.4856v2 [cond-mat.mes-hall] 29 Aug 2012

In a pioneer experiment, Bohlein et al. realized the controlled sliding of two-dimensional colloidal crystals over laser-generated periodic or quasi-periodic potentials. Here we present realistic simulations and arguments which besides reproducing the main experimentally observed features, give a first theoretical demonstration of the potential impact of colloid sliding in nanotribology. The free motion of solitons and antisolitons in the sliding of hard incommensurate crystals is contrasted with the soliton-antisoliton pair nucleation at the large static friction threshold $F_{\rm s}$ when the two lattices are commensurate and pinned. The frictional work directly extracted from particles' velocities can be analysed as a function of classic tribological parameters, including speed, spacing and amplitude of the periodic potential (representing respectively the mismatch of the sliding interface, and the corrugation, or "load"). These and other features suggestive of further experiments and insights promote colloid sliding to a novel friction study instrument.

colloids | friction | solitons | superlubricity | commensurate-incommensurate

The intimate understanding of sliding friction, a central player in the physics and technology of an enormous variety of systems, from nanotribology to mesoscale and macroscale sliding [1, 2], is historically hampered by a number of difficulties. One of them is the practical inaccessibility of the buried interface between the moving bodies – with few exceptions, we can only hypothesize about its nature and behavior during sliding. Another is the general impossibility to fully control the detailed nature, morphology, and geometric parameters of the sliders; thus for example, even perfectly periodic, defect-free contacting surfaces have essentially only been accessible theoretically. If we knew and, on top of that, if we could control the properties and the relative asperity parameters of the sliders, our physical understanding could greatly increase, also disclosing possibilities to tune friction in nano and mesoscopic systems and devices. As Bohlein *et al.* [3] showed, two dimensional (2D) colloid crystalline monolayers can be forced by the flow of their embedding fluid to slide against a laser-generated static potential mimicking the interface "corrugation" potential in ordinary sliding friction. The external pushing force, the interparticle interactions, and especially the corrugation potential are all under control, the latter ranging from weak to strong, and from periodic, to quasi-periodic [4, 5], in principle to more complex types too. Contrary to established techniques in meso and nanosize sliding friction (Atomic Force Microscope, Surface Force Apparatus, Quartz Crystal Microbalance) [6], which address the tribological response in terms of averaged physical quantities (overall static and kinetic friction, mean velocities, slip lengths and slip times, etc.), in colloid sliding every individual particle can in principle be followed in real time, stealing a privilege hitherto restricted to the ideal world of molecular-dynamics (MD) simulations [7, 8, 9].

Materializing concepts long-anticipated theoretically [10, 11], the colloid sliding data showed how the sliding of a flat crystalline lattice on a perfectly periodic substrate takes place through the motion of soliton or antisoliton superstructures (also known in one dimension – 1D – as kinks or antikinks) – positive or negative density modulations that reflect the misfit dislocations of the two lattices that are incommensurate in their mutual registry. While forming regular static Moiré superstructure patterns when at rest, solitons constitute the actual mobile entities during depinning and sliding, and are essential for "superlubricity" [12] – i.e., zero static friction – of hard incommensurate sliders. When solitons are absent at rest owing to commensurability of the two sliders (or are present but pinned in soft incommensurability), the colloids and the periodic potential are initially stuck together. Only after the static friction force $F_{\rm s}$ is overcome, solitons appear (or depin if they already exist but are pinned) unlocking the colloids away from the corrugation potential, so that sliding can take place.

Our aim here is to understand and demonstrate, based on molecular dynamics (MD) sliding simulations, how the great colloid visibility and controllability can be put to direct use in a tribological context. The full phase diagram versus colloid density and sliding force is explored first of all, highlighting a large asymmetry between solitons and antisolitons, and a strong evolution from commensurate to incommensurate caused by sliding. We then extract and predict the frictional work as a function of mean velocity and corrugation amplitude, loosely mimicking "load" – the same variables of classic macroscopic friction laws. We also discuss new local phenomena underlying depinning, including the edge-originated spawning of incommensurate antisolitons and the bulk-originated nucleation/separation of soliton-antisoliton pairs in the commensurate case, as well as global analogies to driven Josephson junctions, charge-density waves, and the sliding of adsorbate islands on crystal surfaces [13, 14, 15, 16, 17, 18, 19].

Modeling and simulations

The driven colloids are modelled as charged point particles undergoing overdamped 2D planar dynamics under an external force F, parallel to the plane, applied to each colloid. While the fluid is not described explicitly, F is to be interpreted as ηv_d where η and v_d are the effective fluid viscosity and velocity. Particles repel each other with a screened Coulomb in-

Reserved for Publication Footnotes

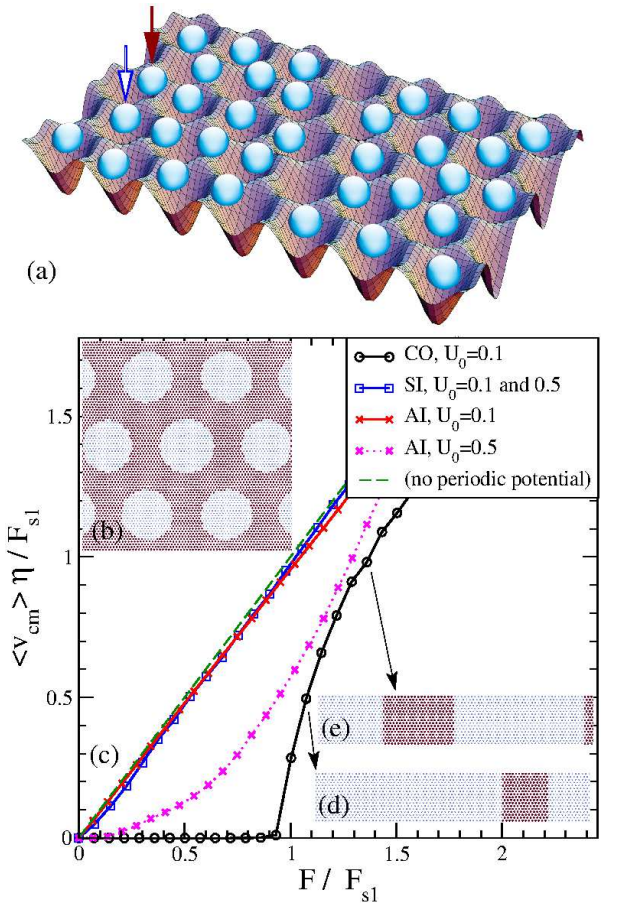

Fig. 1. (a) A sketch of the model for the colloid particles interacting with a periodic potential W. (b) The static initial configuration at $\rho = 0.95$. Three families of antisoliton lines (darker areas) cross at 120 degrees. (c) Velocity-force characteristics for various colloid densities, with a lattice-potential corrugation commensurability ratio $\rho = a_{\rm las}/a_{\rm coll} = 1.0$ (CO), 1.05 (SI), and 0.95 (AI). The CO case always displays static friction. For weak corrugation ($U_0 = 0.1$), $F_{\rm s} = 0$ in both AI and SI incommensurate cases. At larger corrugation ($U_0 = 0.5$) a major asymmetry appears between the AI and SI configurations: only the AI case exhibits a finite depinning threshold with static friction. (d,e) Snapshots of the central region of the initially commensurate colloid during motion, illustrating sliding-generated solitons, whose density increases as F is increased. In all snapshots, colloids located at repulsive spots of the corrugation potential [defined by $W(\mathbf{r}) > -U_0/2$, e.g. the colloid pointed at by the red filled arrow in panel (a)] are drawn as dark red spots, while colloids nearer to potential minima [$W(\mathbf{r}) \leq -U_0/2$, e.g. the colloid pointed at by the blue empty arrow in panel (a)] are light blue.

terparticle repulsion, $V(r_{ij}) = Q/r_{ij}\,\exp(-r_{ij}/\lambda_D)$ with λ_D substantially smaller than the mean distance between particles. Colloids are immersed in a Gaussian-shaped overall confining potential $G(|\mathbf{r}|) = -A_c \exp(-r^2/\sigma^2)$ – the large radius σ representing the laser spot size – and in a triangular-lattice periodic potential $W(\mathbf{r}) = -(2U_0/9)[3/2 + 2\cos(2\pi r_x/a_{\rm las})\cos(2\pi r_y/(\sqrt{3}a_{\rm las})) + \cos(4\pi r_y/(\sqrt{3}a_{\rm las}))]$ representing the interface "corrugation", see Fig. 1a. Finally, in addition to the external force, a Stokes viscous force $-\eta\,\mathbf{v}_i$ acts on each particle $i = 1, ..., N$, and accounts for the dissipation of the colloids kinetic energy into the thermal bath. We typically simulate $N \simeq 30,000$ – a particle number much smaller than in experiment, but sufficient to extract reliable physical results.[1] In the absence of corrugation ($U_0 = 0$), colloids form a 2D crystalline island at rest. The 2D density of the triangular 2D lattice is fixed by N and by the balance of the confining energy G and the 2-body repulsion energy. We

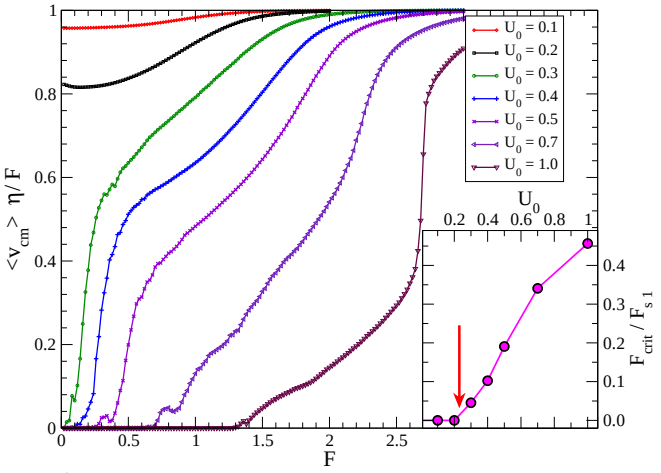

Fig. 2. 2D Aubry transition for antisolitons at $\rho = 0.95$, in an infinite-size colloid system. Main panel: colloid mobility as a function of the applied force, for increasing corrugation amplitude U_0. Note the appearance of pinning with static friction just above U_0= 0.2. Inset: static friction (depinning) force $F_{\rm s}$, normalized to the single-colloid force barrier $F_{s\,1}$, as a function of U_0, with an arrow indicating the critical Aubry corrugation.

set this balance so that the average colloid lattice spacing $a_{\rm coll}$ (before submittal to the corrugation potential W) is unity.[2] We then realize a variety of mismatched ratios $\rho = a_{\rm las}/a_{\rm coll}$ by changing the corrugation period $a_{\rm las}$. In the following, we focus on three representative cases, namely: underdense, $\rho = 0.95$ (antisoliton-incommensurate – AI; the starting state at rest is shown in Fig. 1b); ideally dense, $\rho = 1.0$ (nearly commensurate – CO, which becomes exactly commensurate after turning on W); overdense, $\rho = 1.05$ (soliton incommensurate – SI) [3]. In order to simulate experiment, and also to prevent solitons from leaving the finite-size sample, our external force F is ramped in time in small well-spaced steps, so that its overall value slowly alternates in sign, forth and back with a long time period. Full simulation details are given in the supporting information.

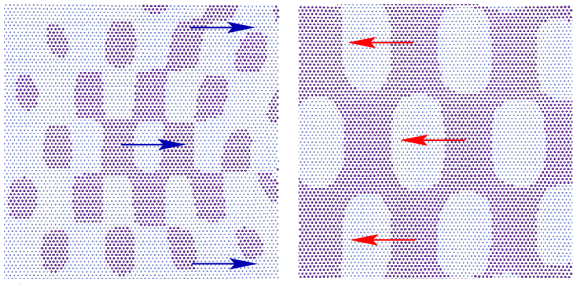

Fig. 3. Depinned, moving particles (darker) of a 2D colloid in a periodic potential under the action of a rightward force F. (a) Rightward propagating solitons of overdense colloids ($\rho = 1.05$, SI); (b) Leftward propagating antisolitons of underdense colloid ($\rho = 0.95$, AI).

[1] To reduce simulation sizes and times, our particles form an island near the center of the Gaussian potential, which is the region experimentally visualized. Particles outside this region, whose role is less relevant, are omitted. Moreover, thermal effects (although straightforward to introduce in simulation), have not been accessed in colloid experiments. After verifying that the main features are not washed out at 300 K (see supporting information), here we will, for the sake of clarity, only present results obtained with a dissipative $T = 0$ Langevin dynamics.

[2] The spacing of the fully relaxed colloid configuration varies smoothly from $a \simeq 0.984$ at the sample center to $a \simeq 1.05$ at the side, with an average density equal to that of a triangular crystal of spacing $a_{\rm coll} = 1$.

[3] Similar models were studied in the past with a view to understand two dimensional Frenkel-Kontorova models and adsorbate monolayers physics [20, 21, 22, 23]

Results

Figure 1c displays the mean speed $\langle v_{\rm cm}\rangle$ of the central portion of the colloid system as a function of the driving force F. Fully reproducing experiment [3], the simulated force-velocity characteristics of Fig. 1c show a large static friction force threshold in the $\rho \simeq 1$ CO case, where the colloid and corrugation lattices are pinned together. Static friction is lost in case of incommensurability and moderate corrugation, where preformed mobile solitons or antisolitons are present. The snapshots of Fig. 3 illustrate the patterns of solitons/antisolitons sliding in opposite directions under the same driving force $F > 0$. For a weak external force and a $\sim 5\%$ lattice mismatch, the static friction drops essentially to zero, and a nearly free viscous sliding is realized, reflecting a situation of "superlubricity" [24, 25, 26]. However, under the same conditions, not all incommensurate geometries are superlubric. Whereas for weak corrugation the overall colloid mobility $\langle v_{\rm cm}\rangle/F$ is remarkably constant for both incommensurate densities, we find in fact that by increasing the corrugation amplitude U_0 the mobility of the AI configuration drops to zero at small force, and pinning with static friction reemerges despite incommensurability. By contrast, SI configurations remain superlubric up to much larger U_0.

The Aubry transition. Borrowing results of the 1D Frenkel Kontorova (FK) model [10], the single-soliton width $d \simeq g^{1/2} a_{\rm las}$ where $g = \xi a_{\rm las}^2 k/U_0$ [here $k = V''(a_{\rm coll})$ and ξ is a constant of order unity] is large for a hard layer on a weak corrugation, and small for a soft layer on a strong corrugation. Between these two extremes, the 1D incommensurate FK model crosses the so-called Aubry transition [24] where superlubricity is lost, and pinning sets in with static friction despite incommensurability. Even in the present 2D case it is qualitatively expected that all incommensurate colloids, both underdense ($\rho \lesssim 1$) and overdense ($\rho \gtrsim 1$) will undergo an Aubry-like superlubric-to-pinned transition for increasing corrugation.

This expectation is confirmed in our 2D model colloid system. Figure 2 (obtained by independent simulations of the infinite-size system with periodic boundary conditions) shows the Aubry-like pinning transition crossed by an AI ($\rho = 0.95$) underdense colloid at a critical corrugation, here $U_0^{\rm crit} \simeq 0.2 - 0.3$. The threshold Aubry corrugation depends upon ρ, and is much larger for overdense SI than for underdense AI colloids.

Soliton-antisoliton asymmetry. This strong asymmetry of static friction – and of all other properties – between overdense ($\rho \gtrsim 1$) and underdense ($\rho \lesssim 1$) colloids can be rationalized, in the limit of strong corrugation $g \ll 1$, in terms of the large physical difference between solitons, defects formed by lines of lattice interstitials, and antisolitons, lines of vacancies. This asymmetry remains even for weak corrugation ($g \gg 1$), when solitons/antisolitons involve relative displacements far smaller than those of proper interstitials or vacancies. A small variation δ in the inter-colloid separation a is sufficient to produce a large relative variation of the effective spring constant, i.e. the interaction curvature

$$\frac{V''(a \pm \delta)}{V''(a)} \simeq \frac{V(a \pm \delta)}{V(a)} \simeq \exp(-\delta/\lambda_D). \qquad [1]$$

For a realistic $\lambda_D = 0.03\, a_{\rm coll}$, this highly nonlinear and asymmetric relation, implies a huge 460% increase whenever two colloids are approached by 5% of their average separation, but only a 82% reduction for a 5% increased separation. This asymmetry is held responsible for the much weaker propensity of solitons to become pinned and to localize compared to antisolitons.

The sliding state. Under sliding, the shapes and geometries of solitons/antisolitons and their motion are of most immediate interest, as they are directly comparable with experiment.

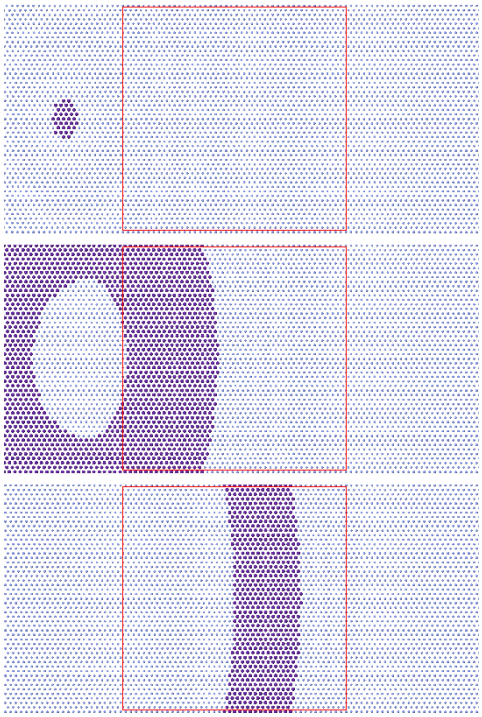

Fig. 4. Three successive snapshots of the initial depinning instants of the commensurate ($\rho = 1$) configuration for the $F \simeq F_{s\,1}$ simulation, see Fig. 1. The horizontally extended window visualizes the the nucleation and separation of a soliton-antisoliton pair, left of the central observation region (square). Pair nucleation constitutes the depinning mechanism of all commensurate sliders.

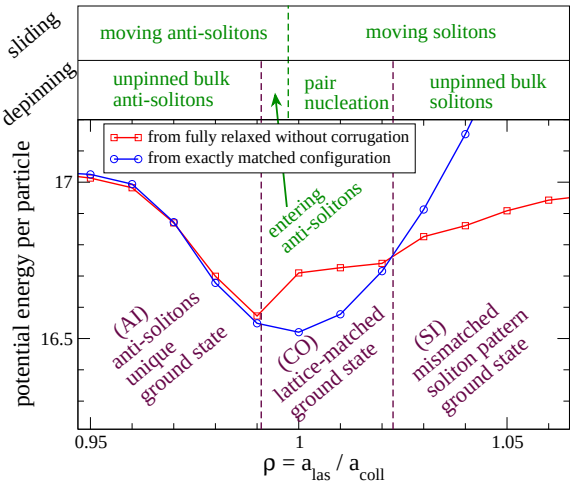

Fig. 5. Effective "phase diagram" of the finite colloid crystal as a function of the lattice spacing mismatch ρ, for $U_0 = 0.1$. The two potential energy curves (colloid-colloid repulsion plus W interaction) characterize the static phases: (red squares) relaxation started from the slightly inhomogeneous configuration produced by a previous relaxation for $U_0 = 0$; (blue circles) relaxation started with a fully matched lattice of spacing $a_{\rm las}$. Two AI (underdense) and SI (overdense) phases surround a commensurate phase (CO). The depinning mechanisms and the soliton structures sustaining sliding are illustrated at top of figure for the different regions.

Figure 3 shows the large-scale checkerboard structure of solitons/antisolitons of the sliding colloid lattice. They move with a speed v much larger than the average lattice speed $\langle v_{\rm cm}\rangle$, because $v/\langle v_{\rm cm}\rangle \sim \rho/(\rho-1)$ by particle conservation. The moving structure is a distortion of the original triangular soliton/antisoliton pattern (Fig. 1b) induced by the circular shape of the confining potential, and by the directional sliding. With increasing F, the soliton arrangements elongate into a stripe-like pattern perpendicular to the driving direction. Comparison with experimental pictures is quite realistic, especially when focusing (as done in experiment) on the central sample region, far from boundaries.

In the AI superlubric colloid $\rho \lesssim 1$, preformed antisolitons fly (leftward) across the colloid lattice antiparallel to the (rightward) force. They are eventually absorbed at the left edge boundary, while new ones spawn at the right edge boundary to replace them, sustaining a steady-state mobility. In the SI superlubric colloid $\rho \gtrsim 1$ conversely, preformed solitons fly rightward, parallel to the force. Solitons, unlike antisolitons, are not automatically spawned at the boundary, owing to the decreasing density. Instead, an antisoliton/soliton pairs must nucleate first, near the boundary, and this is possible only if the force overcomes the nucleation barrier. Below this threshold, we observe that a steady DC external force eventually sweeps out all the preformed solitons transforming the colloid to an artificially pinned, immobile CO state.

Finally, the pinned CO colloid $\rho \gtrsim 1$ only moves after static friction is overcome. As illustrated in Fig. 4, motion starts off here by nucleation of soliton-antisoliton pairs inside the bulk – here close to the left edge because the central region tends to be slightly overdense. The antisolitons flow leftwards and are absorbed by the left edge, becoming undetectable to the optically monitored central part of the colloid, where only solitons transit, as seen in experiment. This type of commensurate nucleation has been described in considerable detail in literature, including finite-temperature effects [11, 27]. We note here that in the pinned CO colloid the soliton or antisoliton density, initially zero, actually increases with increasing sliding velocity (see, e.g., Fig. 1d,e), as opposed to frankly incommensurate cases, where it is nearly constant.

Phase-diagram evolution with sliding. Much can be learned about the habit of sliding colloids from their behavior and their structural phase diagram, first at rest and then under sliding. With $\rho \simeq 1$, close to commensurate but not exactly commensurate, the colloid monolayer can realize in the periodic potential two alternative static arrangements which are local minima of the overall free energy: a fully lattice-matched CO state, or a weakly incommensurate state characterized by a sparse soliton (AI or SI) superstructure, with a density fluctuating around the local value prescribed by the $G-V$ balance. Comparing the potential energy of these two states as a function of ρ, the static phase diagram contains, as sketched in Fig. 5, a fully commensurate extended CO region separated from the AI and SI regions by commensurate-incommensurate transitions, well known in adsorbed surface layers [28, 29, 30, 31]. The CO region is wider on the SI side ($\rho > 1$) than the AI side ($\rho < 1$), another manifestation of the SI-AI asymmetry discussed above. The CO range naturally widens or shrinks when the corrugation amplitude U_0 is increased or decreased.

Under an external force F, sliding effectively tilts the balance between the two static phases (loosely speaking, for of course under sliding the physical significance of a "phase" is not the same as at rest) sliding populates the former CO phase with solitons/antisolitons, turning it effectively into SI or AI. In the running state, the colloid average density increases or decreases from 1 to a value closer to the nominal ρ of the colloid at $U_0 = 0$. This explains why in a quasi-commensurate configuration with $\rho \gtrsim 1$ such as that shown by Bohlein *et al.* [3], solitons (and not, e.g., soliton-antisoliton pairs) sweep the colloid upon depinning, as also seen in Fig. 1d,e.

It is curious to note here the different fate of solitons in the slightly overdense CO and in the SI phases. In the CO phase they do not exist at rest, but they appear after depinning and under sliding. In the SI phase they exist at rest, but they could be swept out under DC sliding, when a weak external force can turn the SI colloid into effectively CO. We never saw this sweepout phenomenon on the AI side.

Frictional analysis

We turn now to frictional work, a quantity of crucial importance for the tribological significance of colloid sliding. We can write the overall power balance as the scalar product of the instantaneous velocity $\mathbf{v}_i$ of each colloid i by the net force acting on it, $\eta\,(\mathbf{v}_d - \mathbf{v}_i)$, including both the bare external force $\mathbf{F} = \eta\mathbf{v}_d$ and the viscous drag $-\eta\mathbf{v}_i$. This product vanishes instantaneously at any time when either colloids are stuck ($\mathbf{v}_i = \mathbf{0}$) or else when the corrugation potential is absent, so that $\mathbf{v}_i \equiv \mathbf{v}_d$. After averaging over a very long trajectory, the balance reads

$$\begin{aligned} P_{\rm tot} &= \sum_i \eta\langle(\mathbf{v}_d - \mathbf{v}_i)\cdot\mathbf{v}_i\rangle \\ &= \left(N\mathbf{F}\cdot\langle\mathbf{v}_{\rm cm}\rangle - \eta\langle|\mathbf{v}_{\rm cm}|^2\rangle\right) - \eta\sum_i\langle|\mathbf{u}_i|^2\rangle \\ &= P_{\rm frict} - P_{\rm kin}\,, \end{aligned} \qquad [2]$$

where $\mathbf{u}_i = \mathbf{v}_i - \mathbf{v}_{\rm cm}$. Under steady-state sliding conditions where $P_{\rm tot} = 0$, the effective friction power $P_{\rm frict}$ is exactly balanced by an internal kinetic energy excess rate. Per colloid particle, $P_{\rm frict}$ is

$$p_{\rm frict} = \frac{P_{\rm frict}}{N} \simeq \mathbf{F}\cdot\langle\mathbf{v}_{\rm cm}\rangle - \eta|\langle\mathbf{v}_{\rm cm}\rangle|^2, \qquad [3]$$

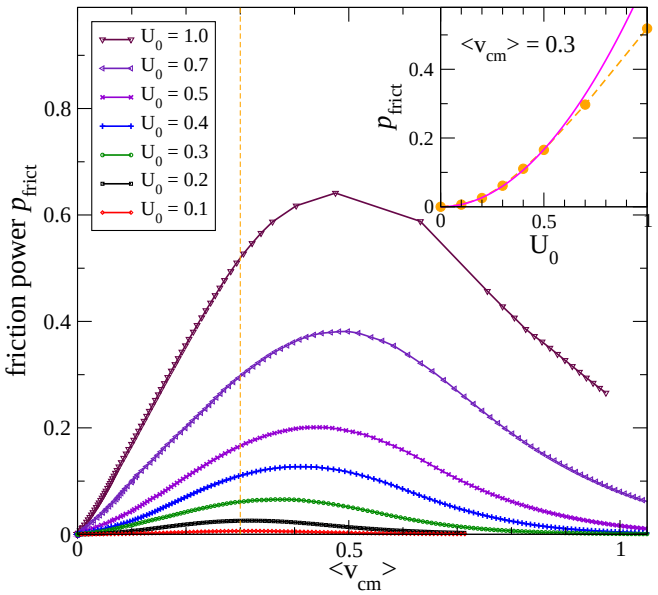

Fig. 6. Sliding friction $p_{\rm frict}$ per particle as a function of speed $\langle v_{\rm cm}\rangle$ for an underdense AI colloid $\rho = 0.95$ for increasing corrugation amplitude U_0. Inset: U_0 dependence of friction for speed $\langle v_{\rm cm}\rangle = 0.3$, showing the quadratic rise for weak corrugation behavior, followed by a roughly linear growth.

where small center of mass fluctuations are neglected, by assuming $\langle \mathbf{v}_{\rm cm}{}^2 \rangle \simeq |\langle \mathbf{v}_{\rm cm} \rangle|^2$.

Figure 6 shows $p_{\rm frict}$ (briefly referred to as "friction" in the following) for the special case of the AI underdense phase as extracted as a function of $\langle \mathbf{v}_{\rm cm} \rangle$ through a "bulk" simulation (with periodic boundary conditions as in Fig. 2). The main features found are (i) a linear rise at low CM speed; (ii) a decline at large speed; (iii) a maximum at some intermediate corrugation-dependent speed. We moreover observe that (iv) the dissipated power increases (not unexpectedly) with corrugation; and (v) the corresponding frictional maximum simultaneously shifts to larger speed.

The qualitative interpretation of these results is relatively straightforward, and yet revealing. (i, iv) At low sliding velocities the motion of solitons/antisolitons involves the viscous motion of individual particles with a velocity distribution whose spread toward higher values rises proportionally to the sliding speed and inversely proportional to their spatial width. As shown, e.g. within the 1D FK model [10], but also in the present simulations, the width d of solitons/antisolitons increases roughly as $d \sim a_{\rm las}\sqrt{g}$ with the dimensionless interparticle interaction strength $g \propto a_{\rm las}^2 V''(a_{\rm coll})/U_0$ measured relative to the periodic corrugation amplitude. The decrease in width with increasing corrugation U_0 requires an increasing instantaneous speed of individual particles in the soliton/antisoliton, yielding an increasing viscous friction, and a decreasing overall mobility as observed. (ii, iii, v) At high sliding velocities, the colloid relaxation time exceeds the soliton/antisoliton transit time across the Peierls-Nabarro barrier [10] so that their spatial structure is gradually washed out by the sliding motion. The critical speed where the smoothening behavior takes over, roughly corresponding to maximal friction, increases as corrugation increases, corresponding to narrower solitons/antisolitons that are harder to wash out. The increase of friction with corrugation strength U_0, plotted in the inset for a chosen speed, is found to be quadratic at weak corrugation, gradually turning to linear for larger values. Linear response theory naturally accounts for the quadratic increase, a behavior first discussed by Cieplak *et al.* [32] and observed in quartz crystal microbalance experiments [33].

Demonstrated for a specific AI case with antisolitons, the above results appear in fact of general validity for infinitely extended sliders of controlled colloid density, and apply equally well although with great quantitative asymmetry to SI with solitons, once their larger widths and greater mobilities and weaker Peierls-Nabarro barriers are taken into account.

Summary and Conclusions

In this study we have presented initial simulation results and theory that strongly vouch in favor of sliding of colloid layers on laser-originated corrugations as a promising tool for future tribological advances. The motion of solitons and antisolitons known from experiment is reproduced and understood, unraveling the subtle depinning mechanisms at play. The presence of Aubry transitions is pointed out for future verification, along with a strong asymmetry between underdense and overdense incommensurate layers. Of direct tribological interest, we anticipate the behavior of friction with corrugation (mimicking "load") and with sliding velocity, with results which, while of course generally very different from the classic laws of macroscopic friction, are highly relevant to friction at nano and mesoscopic scales. Our approach moreover indicates a strong complementarity between theory plus simulation, and experiment, an aspect which we intend to pursue further.

There are many lines of future research that this study implicitly suggests. One line will be to pursue the analogy of the sliding over a periodic potential with other systems such as driven Josephson junctions [34], and sliding charge-density waves [14]. Time-dependent nonlinear phenomena such as the Shapiro steps [14, 34] should become accessible to colloid sliding too. A second line is to include non-periodic complications to the corrugation potential, including the quasicrystal geometry such as that recently realized [35] and beyond that, random, or pseudo-random corrugations to be realized in the future. A third line involves the investigation of the lubricant speed quantization phenomena, characterized so far only theoretically [36, 37, 38, 39].

A further very important development will be to address colloidal friction in larger, mesoscopic or macroscopic size systems, whose phenomenology is accessible so far only by a few, very ingenious, but very limited, methods [6, 16, 17, 40, 41, 42]. A major scope in that case will be to realize and study stick-slip friction and aging phenomena, at the heart of realistic physical and technological tribology.

ACKNOWLEDGMENTS.

This work is partly funded by the Italian Research Council (CNR) via Eurocores FANAS/AFRI, by the Italian Ministry of University and Research through PRIN projects 20087NX9Y7 and 2008y2p573, and by the Swiss National Science Foundation Sinergia CRSII2_136287.

1. Vanossi A, Manini N, Urbakh M, Zapperi S, Tosatti E (2011) Modeling friction: from nano, to meso scales. http://arxiv.org/abs/1112.3234.
2. Urbakh M, Klafter J, Gourdon D, Israelachvili J (2004) The nonlinear nature of friction. Nature (London) 430:525-528.
3. Bohlein T, Mikhael J, Bechinger C (2012) Observation of kinks and antikinks in colloidal monolayers driven across ordered surfaces. Nature Mater 11:126-130.
4. Mikhael J, Roth J, Helden L, Bechinger C (2008) Archimedean-like tiling on decagonal quasicrystalline surfaces. Nature (London) 454:501-504.
5. Mikhael J, Schmiedeberg M, Rausch S, Roth J, Stark H, Bechinger C (2010) Proliferation of anomalous symmetries in colloidal monolayers subjected to quasiperiodic light fields. Proc Natl Acad Sci USA 107:7214-7218.
6. Carpick RW, Salmeron M (1997) Scratching the surface: fundamental investigations of tribology with atomic force microscopy. Chem Rev 97:1163-1194.
7. Vanossi A, Tosatti E (2012) Colloidal friction: kinks in motion. Nature Mater 11:97-98.
8. Reichhardt C, Olson CJ (2002) Novel colloidal crystalline states on two-dimensional periodic substrates. Phys Rev Lett 88:248301.
9. Reichhardt C, Olson CJ (2011) Dynamical Ordering and Directional Locking for Particles Moving over Quasicrystalline Substrates. Phys Rev Lett 106:060603.
10. Braun OM, Kivshar YS (2004) The Frenkel-Kontorova Model: Concepts, Methods, and Applications (Springer-Verlag, Berlin).
11. Braun OM, Bishop AR, Röder R (1997) Hysteresis in the underdamped driven Frenkel-Kontorova model. Phys Rev Lett 79:3692-3695.
12. Superlubricity (2007) ed. by A. Erdemir, J.-M. Martin (Elsevier, The Netherlands).
13. Ustinov AV (1998) Solitons in Josephson junctions. Physica D 123:315-329.
14. Grüner G (1988) The dynamics of charge-density waves. Rev Mod Phys 60:1129-1182.
15. Krim J, Widom A (1988) Damping of a crystal-oscillator by an adsorbed monolayer and its relation to interfacial viscosity. Phys Rev B 38:12184-12189.
16. Krim J, Solina DH, Chiarello R (1991) Nanotribology of a kr monolayer - a quartz-crystal microbalance study of atomic-scale friction. Phys Rev Lett 66:181-184.
17. Tomassone MS, Sokoloff JB, Widom A, Krim J (1997) Dominance of phonon friction for a xenon film an a silver (111) surface. Phys Rev Lett 79:4798-4801.
18. Bruschi L, Carlin A, Mistura G (2002) Depinning of atomically thin Kr films on gold. Phys Rev Lett 88:046105.
19. Bruschi L, Fois G, Pontarollo A, Mistura G, Torre B, de Mongeot FB, Boragno C, Buzio R, Valbusa U (2006) Structural depinning of ne monolayers on Pb at $T < 6.5$ k. Phys Rev Lett 96:216101
20. Lomdahl PS, Srolovitz DJ (1986) Dislocation generation in the two-dimensional Frenkel-Kontorova model at high stresses. Phys Rev Lett 57:2702-2705.
21. Srolovitz DJ, Lomdahl PS (1986) Dislocation dynamics in the 2-d Frenkel-Kontorova model. Physica D 23:402-412.
22. Gornostyrev YN, Katsnelson MI, Kravtsov AV, Trefilov AV (1999) Fluctuation-induced nucleation and dynamics of kinks on dislocation: soliton and oscillation regimes in the two-dimensional Frenkel-Kontorova model. Phys Rev B 60:1013-1018.
23. Braun OM, Paliy MV, Röder J, Bishop AR (2001) Locked-to-running transition in the two-dimensional underdamped driven Frenkel-Kontorova model. Phys Rev E 63:036129.

24. Peyrard M, Aubry S (1983) Critical-behavior at the transition by breaking of analyticity in the discrete Frenkel-Kontorova model. J Phys C: Solid State Phys 16:1593-1608.
25. Dienwiebel M, Verhoeven GS, Pradeep N, Frenken JWM, Heimberg JA, Zandbergen HW (2004) Superlubricity of graphite. Phys Rev Lett 92:126101.
26. Filippov AE, Dienwiebel M, Frenken JWM, Klafter J, Urbakh M (2008) Torque and twist against superlubricity. Phys Rev Lett 100:046102.
27. Reguzzoni M, Ferrario M, Zapperi S, Righi MC (2010) Onset of frictional slip by domain nucleation in adsorbed monolayers. Proc Natl Acad Sci USA 107:1311-1316.
28. Coppersmith SN, Fisher DS, Halperin BI, Lee PA, Brinkman WF (1981) Dislocations and the commensurate-incommensurate transition in 2 dimensions. Phys Rev Lett 46:549-552.
29. Bak P (1982) Commensurate phases, incommensurate phases and the devils staircase. Rep Prog Phys 45:587-629.
30. Patrykiejew A, Sokołowski S, Zientarski T, Binder K (1999) On the commensurate-incommensurate transition in adsorbed monolayers. Surf Sci 421:308-319.
31. Mangold K, Leiderer P, Bechinger C (2003) Phase transitions of colloidal monolayers in periodic pinning arrays. Phys Rev Lett 90:158302.
32. Cieplak M, Smith ED, Robbins MO (1994) Molecular-origins of friction - the force on adsorbed layers. Science 265:1209-1212.
33. Coffey T, Krim J (2005) Impact of substrate corrugation on the sliding friction levels of adsorbed films. Phys Rev Lett 95:076101.
34. Tinkham M (1996) Introduction to Superconductivity (McGraw Hill, New York).
35. Bohlein T, Bechinger C (in print in Phys Rev Lett) Experimental observation of directional locking and dynamical ordering of colloidal monolayers driven across quasiperiodic substrates. arXiv:1206.6018.
36. Vanossi A, Manini N, Divitini G, Santoro GE, Tosatti E (2006) Exactly quantized dynamics of classical incommensurate sliders. Phys Rev Lett 97:056101.
37. Cesaratto M, Manini N, Vanossi A, Tosatti E, Santoro GE (2007) Kink plateau dynamics in finite-size lubricant chains. Surf Sci 601:3682-3686.
38. Vanossi A, Manini N, Caruso F, Santoro GE, Tosatti E (2007) Static friction on the fly: Velocity depinning transitions of lubricants in motion. Phys Rev Lett 99:206101.
39. Castelli IE, Capozza R, Vanossi A, Santoro GE, Manini N, Tosatti E (2009) Tribology of the lubricant quantized sliding state. J Chem Phys 131:174711.
40. Drummond C, Israelachvili J (2001) Dynamic phase transitions in confined lubricant fluids under shear. Phys Rev E 63:041506.
41. Rubinstein SM, Cohen G, Fineberg J (2004) Detachment fronts and the onset of dynamic friction. Nature (London) 430:1005-1009.
42. Rubinstein SM, Cohen G, Fineberg J (2006) Contact area measurements reveal loading-history dependence of static friction. Phys Rev Lett 96:256103.